Proceedings of
ASME TURBOEXPO 2000
May 8-11, 2000, Munich Germany

2000-GT-267

CONTROL OF SEPARATION BUBBLE ON A BLADE LEADING EDGE BY A STATIONARY BAR WAKE

K. Funazaki, Y. Harada and E. Takahashi
Iwate University
Morioka, Japan

ABSTRACT

This paper describes an attempt to suppress a blade leading edge separation bubble by utilizing a stationary bar wake. This study aims at exploration of a possibility for reducing the aerodynamic loss due to blade boundary layer that is accompanied with the separation bubble. The test model used in this study consists of semi-circular leading edge and two parallel flat plates. It can be tilted against the inlet flow so as to change the characteristics of the separation bubble. Detailed flow measurements over the test model are conducted using a single hot-wire probe. Emphasis in this study is placed on the effect of bar shifting or bar clocking across the inlet flow in order to see how the bar-wake position with respect to the test model affects the separation bubble as well as aerodynamic loss generated within the boundary layer. The present study reveals a loss reduction through the separation bubble control using a properly *clocked* bar wake.

INTRODUCTION

Behavior of the separation bubble on the suction surface of a compressor or a turbine blade has been attracting attention of researchers and designers of turbomachines for several decades because the separation is closely related to efficiency, stability, heat transfer and noise generation encountered in turbomachines. Recently much effort is devoted to studies of a leading edge separation bubble. Hazarika and Hirsch (1994)(1995) executed a series of detailed measurements of separation bubble on the leading edge of a rounded flat plate, which revealed the transitional behavior of the separation bubble in addition to the characteristics of the separation bubble in terms of velocity/ turbulence intensity profiles or separation length. Hazarika and Hirsch (1996) also examined the Reynolds number effects upon the separation bubble. Walraevens and Cumptsy (1995) measured pressure distributions and boundary layers around the test models with a circular leading and an elliptic leading edge accompanying the separation bubble. They reported that the leading edge geometry affected the aerodynamic performance of the models through its influence on the separation bubble. Calvert (1994), using a Martensen singularity method combined with a boundary layer code, made a number of calculations of the flow around blade leading edge with various geometries. Calvert compared his numerical results with several experimental data, showing the usefulness and the limitation of his approach to predict the leading edge flows. Malkiel and Mayle (1995) investigated the process of turbulence development in a separation bubble, from which they showed the transition associated with the separation bubble was characterized by an intermediate feature between attached boundary layers and free shear layers.

Meanwhile, a number of attempts have been made to control separation and/or separation bubble on an isolated airfoil using conventional devices such as vortex generators or other devices like acoustic excitation. However, few of these devices were ever applied to turbomachines because they were far from practical in turbomachines or were accompanied with severe penalties in service. In consideration of the flow field inside of the turbomachines, one of the most realistic approaches to control the separation is to utilize various sources of intense turbulence inherent in the turbomachines, such as stationary or unsteady wakes coming from upstream blade rows. Cumpsty et al. (1995) investigated the effects of periodic wake passing over separated boundary layers on a compressor blade, indicating the important role of calmed regions created after wake-induced turbulence patches in suppressing the separation bubble. Schulte and Hodson (1998) developed a model to predict the calmed region effect upon transitional behavior of boundary layers on LP turbine blades, which showed the calmed region was less prone to separation than a conventional laminar boundary layer. In the above-mentioned studies, main focus was on the effect of the moving wakes from the adjacent blade row. As for the effect of stationary wakes, Kyriakides et al. (1999) examined effects of a stationary bar wake upon laminar-turbulent transition on a flat-plate boundary layer. They found that the vortical structure of the wake affected the transitional behavior of the boundary layer even before the wake directly contacted the boundary layer. Recently much concern has arisen about a technique for improving stage efficiency that changes the interaction between upstream stator wakes and the downstream stator vanes of concern by shifting the upstream stator vanes in the circumferential direction. This technique is frequently called ‘airfoil clocking’ or 'airfoil indexing', and several researchers have examined to what extent the technique could improve the stage efficiency (Huber et al. (1996), Griffin et al. (1996), Gundy-Burlet et al. (1997), Walker et al. (1998)). They found that some configurations could maximize the stage efficiency, although the mechanism of the clocking was not fully understood yet. A similar approach with the airfoil clocking technique seems to be applicable and practical in controlling the separation and/or separation bubble encountered in turbomachines because it does not require any extra devices for the purpose.

This study shows an attempt using the wake from a stationary bar to minimize aerodynamic loss associated with a separated boundary layer on a large-scaled blunt airfoil that is a model of the leading edge portion of actual airfoils. In this study the bar is transversely shifted (or ‘clocked’) so that the bar wake interacts with the boundary layer on the test model in different manners. Detailed measurements by use of a hot-wire probe reveal that it is possible to reduce the boundary layer loss by positioning the wake-generating bar at a proper location.

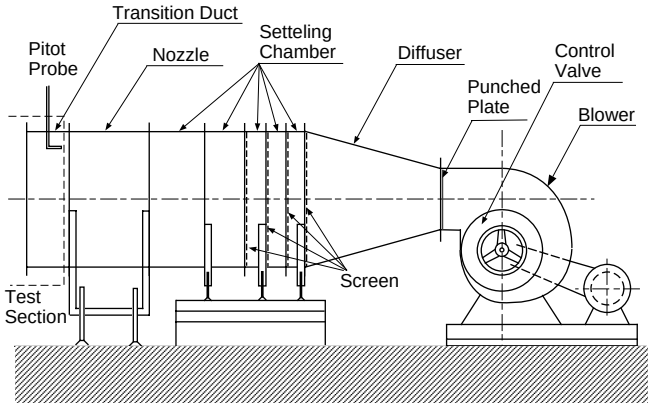

Figure 1 Test facility

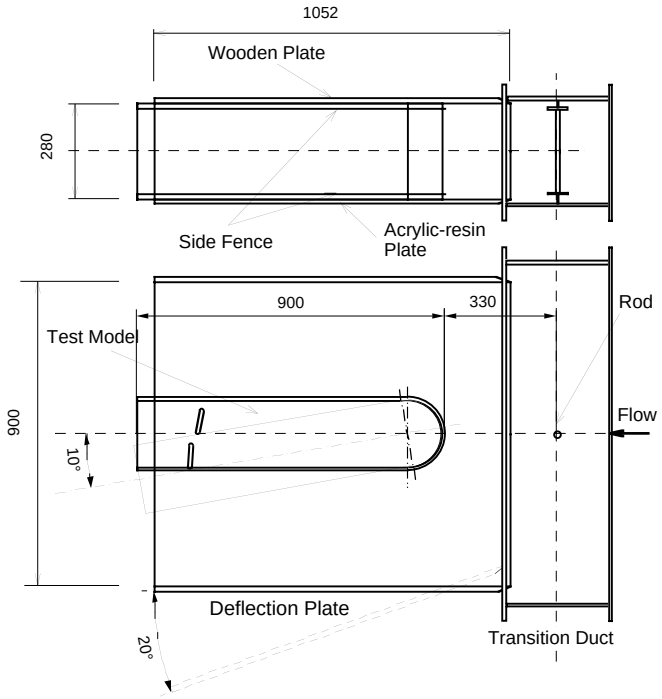

Figure 2 Test section with the test model (unit in mm)

NOMENCLATURE

$b_{1/2}$	: semi-depth width of the wake velocity profile [m]
C_d	: drag coefficient of the bar
C_p	: pressure coefficient ($=\left(P_0 - p\right)\big/\rho U_{in}^2/2$)
D	: diameter of the test model leading edge [m]
d	: diameter of the wake-generating bar [m]
h	: distance between the duct centerline and the stagnation streamline [m]
i	: incidence [deg]
P_0, p	: inlet stagnation pressure, static pressure [Pa]
R	: radius of the test model leading edge
Re	: Reynolds number ($= U_{in}D/\nu = 1.3\times10^5$)
$Tu_{\max}$	: peak value of the wake profile
$Tu(Y)$	: bar wake turbulence profile
Tu_∞	: turbulence intensity ($= u'/U_{in}$)
s	: distance from the stagnation streamline [m]
$U(x_s)$	: velocity on the model surface
U_{in}	: inlet velocity [m/s]

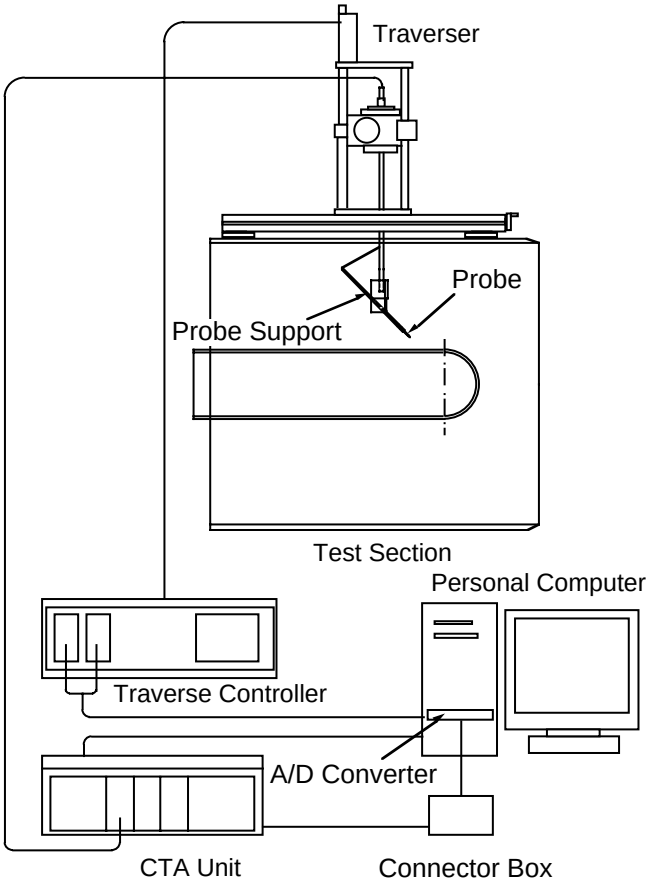

Figure 3 Measurement system using a hot-wire probe

$\bar{u}$, u'	: averaged velocity, standard deviation of the velocity [m/s]
X	: longitudinal distance from the model leading edge
x_s	: surface length measured from the model leading edge [m]
Y	: distance from the duct centerline [m]
y	: distance from the flat plate of the test model [m]
δ^*	: displacement thickness [m]
δ_3	: energy dissipation thickness [m]
ν	: kinematic viscosity [m^2/s]
θ	: momentum thickness [m]
ρ	: density [kg/m^3]
ζ	: loss index

EXPERIMENTAL DETAIL

Test Facility

Figure 1 shows the test facility in this study. Air from the blower passed through the diffuser and the settling chamber with several screens, while the flow rate was adjusted by the inlet valve. The transition duct was attached to the exit of the nozzle of 10:3 contraction ratio. Because a large-scaled test model was adopted in this study for the purpose of detailed measurements of a separated boundary layer, the nozzle contraction ratio was eventually of less moderate value. Accordingly, turbulence intensity of the flow remained to be about 1% at the inlet of the test section.

Test Model

Figure 2 exhibits the test duct, in which the test model was contained. The test duct, 0.9 [m] height and 0.28 [m] width, consisted of a wooden and an acrylic-resin side plates in conjunction with two

moveable top and bottom plates. The test duct with sharp-edged inlet was inserted into the transition duct and some amount of the flow was discharged from the gap between the test duct and the transition duct, from which boundary layers on the sidewall of the duct restarted. The test model contained a semi-circular cylinder and two parallel flat plates, all of which were made from acrylic-resin. The model located in the middle of the duct. The model was 0.9 [m] long and 0.28 [m] wide, the diameter of its leading edge D being 0.2 [m]. This large size of the model enabled the detailed measurements of the separation bubble on the test model. However, it could not be helped that the flow field around the test model, and accordingly the separation bubble, was influenced by the upper or the lower plate of the duct. Besides, to minimize the side wall effect upon the boundary layer over the test model, two side fences were attached to the surface of the model near the both sidewalls where the spacing between the fence and the side plate was 0.015 [m]. The height and the thickness of the fence was 0.01 [m] and 0.001 [m], respectively. The model had a number of pressure holes on its surface staggering around the model centerline.

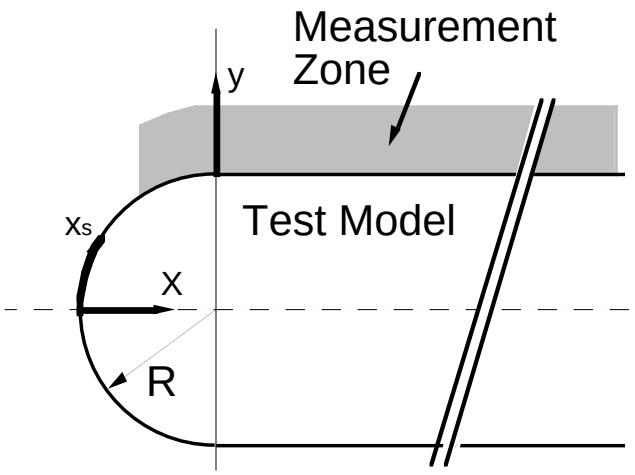

Figure 4 Attachment for the measurement of the boundary layers at two separated locations

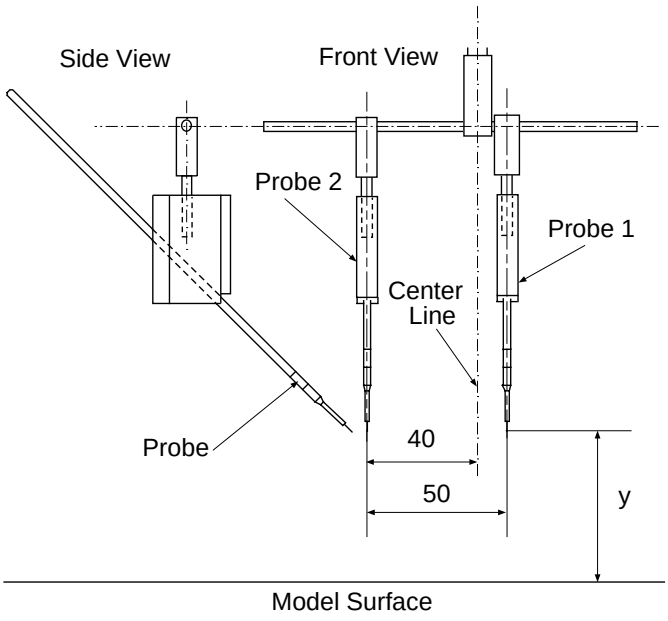

Figure 5 Attachment for the measurement of the boundary layers at two separated locations

It was possible to tilt the model with respect to the inflow direction to change the incidence of the model i by $\pm$ 10 [deg]. In that case the top and the bottom plates were also inclined to adjust a pressure distribution over the test model, as shown in Figure 2.

As a wake generator, a circular cylinder of 0.01 [m] diameter and 0.3 [m] length was used in this study. This bar had two rings near the both ends to keep the wake flow as two-dimensional as possible, and located 0.33 [m] upstream of the test model. Since the cylinder was fixed to the side walls of the transition duct with two bolts, it was easy to shift transversely (or 'clock') the bar-wake by changing the vertical position of the cylinder from the duct centerline.

Measurement System

Velocity Measurements Figure 3 schematically represents the system for the measurement of a boundary layer using CTA (Constant Temperature Anemomenter). A 3-ch CTA, DANTEC StreamLine, measured the flow velocity around the test model using hot-wire probes, DANTEC 55P11. The measurement system including a traverse unit was almost fully controlled by the software, DANTEC StreamWare, running on a PC equipped with an A/D board (National Instruments). Data sampling frequency was 10kHz and one record size was 2^{14}. A temperature probe monitored the flow temperature, which was also used to compensate the acquired velocity signal for the flow temperature variation. The probe was calibrated inside the test duct, and a curve fitting using 4-th order polynomial yielded the relationship between the flow velocity and the output voltage.

As shown in Figure 3, the traverse unit vertically moved the probe to a specified position with accuracy of $\pm$ 0.05 [mm], where the probe was inclined by 45 [deg] from the vertical to reduce the probe blockage effect on the flow. Figure 4 displays the area to be measured by the hot-wire probe, with some explanations on the coordinate system or variables used in this study. The area extended from x_s/R = 0.96 to x_s/R = 3.49 and from y/R = 0.003 to y/R = 0.5. As indicated in Figure 4, the probe moved towards the y-direction, not the normal direction to the test surface, in the measurement over the semi-circular leading edge. The level of the traverse unit was paralleled to the flat portion of the test model even in the non-zero incidence cases by adjusting the legs of the traverse unit. A custom-made height gage on the test model then provided the datum line to ensure the accurate probe-positioning from the surface of the test model. In expectation of two-dimensionality of the flow around the test model, the hot-wire probe measured the boundary layer along the centerline of the test model. In order to check this supposition, boundary layers on two spanwisely-separated locations were also examined at the same time using two hot-wire probes and an attachment as appeared in Figure 5.

Pressure Measurements The pressure holes, connected to pressure transducers with pressure tubes, detected static pressure distributions on the test model. The error of the pressure transducer was about $\pm$ 2.5 [Pa]. A Pitot probe in the transition duct measured a reference inlet velocity U_{in} and inlet stagnation pressure P_0.

Uncertainty Analysis Uncertainty of the velocity measurement using the hot-wire probe originated mainly from the error in the measurement of the reference velocity, which was about $\pm$3%, while the error associated with the curve fitting was less than $\pm$1%. In total the uncertainty of the velocity measurement was about $\pm$3.2%.

Data Reduction

Static pressure measured on the test surface, p, was expressed in terms of pressure coefficient defined as

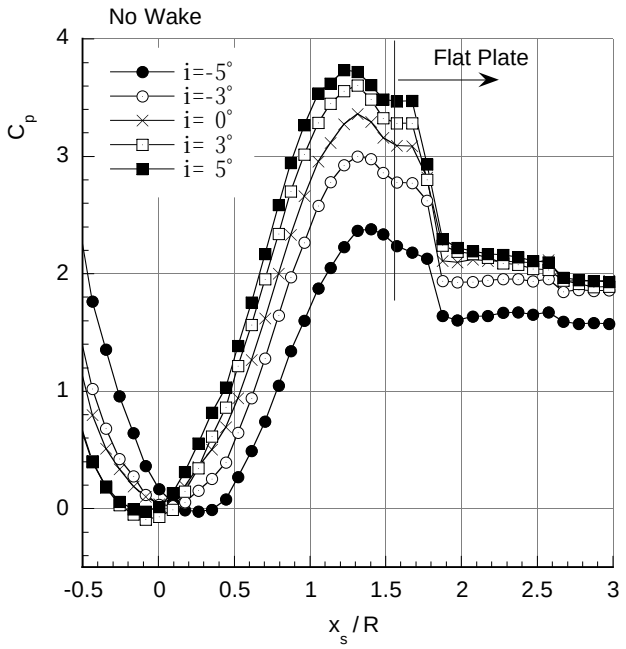

Figure 6 Pressure distributions around the test model for several incidences for no-wake condition

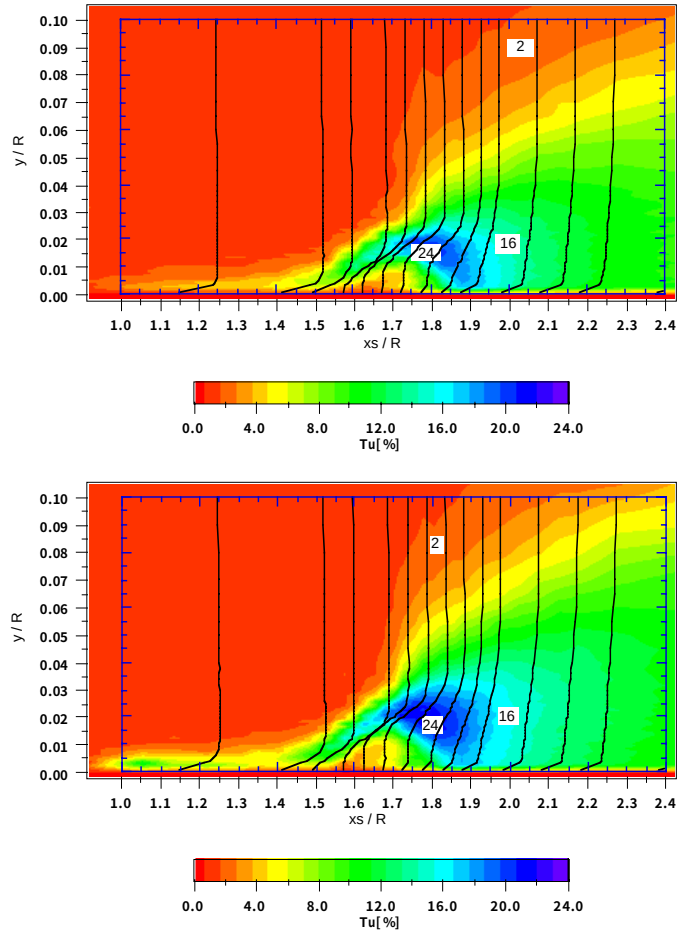

Figure 7 Undisturbed velocity profiles and turbulence intensity contours upper : i = 0 / lower : i = 5

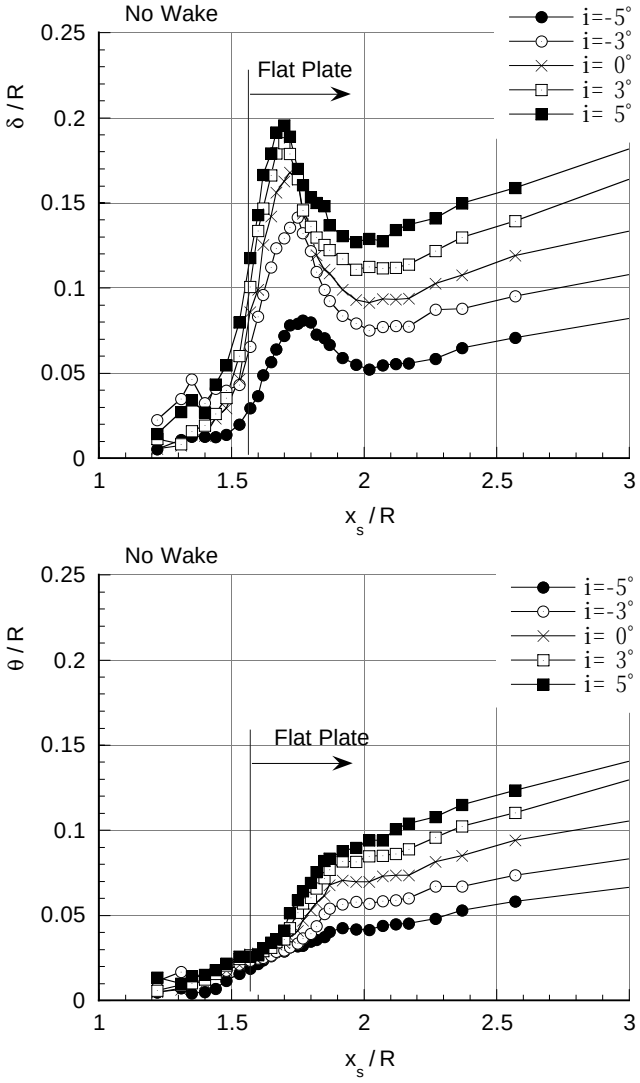

Figure 8 Displacement thickness (upper) and momentum thickness (lower) of the undisturbed boundary layer

$$C_p(x_s) = \frac{P_0 - p}{\rho U_{in}^2/2} = \left(U(x_s)/U_{in}\right)^2. \quad (1)$$

The average and standard deviation of the velocity data measured with the hot-wire probe, $\bar{u}$ and u', were calculated by the following equations, respectively,

$$\bar{u} = \frac{1}{n}\sum_{k=1}^{n} u_k , \quad (2) \quad u' = \sqrt{\frac{1}{n}\sum_{k=1}^{n}\left(u_k - \bar{u}\right)^2} , \quad (3)$$

where $n = 2^{14}$. Turbulence intensity Tu was also defined as

$$Tu = \frac{u'}{U_{in}} . \quad (4)$$

Displacement thickness, momentum thickness and energy dissipation thickness of the boundary layer was given by

$$\delta^* = \int_0^{y_{max}} \left(1 - \frac{\bar{u}}{\bar{u}_{max}}\right) dy , \quad (5)$$

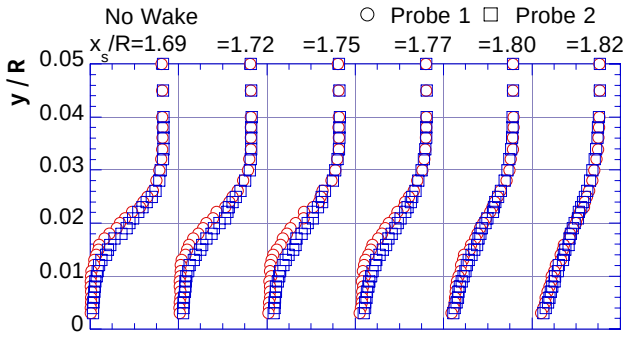

Figure 9 Comparison of velocity profiles measured at two separated locations (no wake condition)

$$\theta = \int_0^{y_{max}} \frac{\bar{u}}{\bar{u}_{max}}\left(1-\frac{\bar{u}}{\bar{u}_{max}}\right)dy, \qquad (6)$$

$$\delta_3 = \int_0^{y_{max}} \frac{\bar{u}}{\bar{u}_{max}}\left(1-\left(\frac{\bar{u}}{\bar{u}_{max}}\right)^2\right)dy, \qquad (7)$$

where y_{max} was the distance from the test surface where the velocity in the boundary layer reached the maximum $\bar{u}_{max}$. In this study the momentum thickness was used for convenience in judging whether the effect of the 'clocked' bar-wake was a useful approach or not for reducing aerodynamic loss associated with the boundary layer. However, since the momentum thickness did not have any direct relation with the loss generation (Cumptsy (1989)), a loss index using the energy dissipation thickness was introduced in the last section of this paper.

RESULTS

Undisturbed Cases

Pressure Distributions Figure 6 are pressure distributions over the test model acquired for several incidences in the no-wake condition, where the abscissa represents the surface length from the geometrical stagnation point for $i = 0$. Looking at the movement of the stagnation point for each case, it turns out that the pressure distributions near the stagnation points did not vary symmetrically with the incidence, despite the symmetric change of the incidence with respect to the centerline. This was due to the restricted movement of the top plate of the test duct in adjusting the flow direction for the negative incidence cases. These pressure distributions, except for i = -5, had plateaux beginning from the location nearby the junction of the semi-circular cylinder and the flat plate, indicating the existence of a separation bubble there. The length of the separation bubble, defined as the distance between the front end of the plateau and the rear end of the abrupt drop in the pressure coefficient, exhibited a slight increase with the incidence.

Velocity and Turbulence Intensity Figure 7 are the data measured for $i = 0$ and $i = 5$ showing undisturbed velocity profiles at several streamwise locations and turbulence intensity distributions. These data clearly exhibit typical features of separation bubble as described by Malkiel and Mayle (1995). The high turbulence intensity area near the wall, in other words shear layer, rose off the wall at $x_s/R \cong 1.5$ for each incidence, taking a bow shape in the main stream. Inflection points of the velocity profiles appeared near the center of the shear layer. The

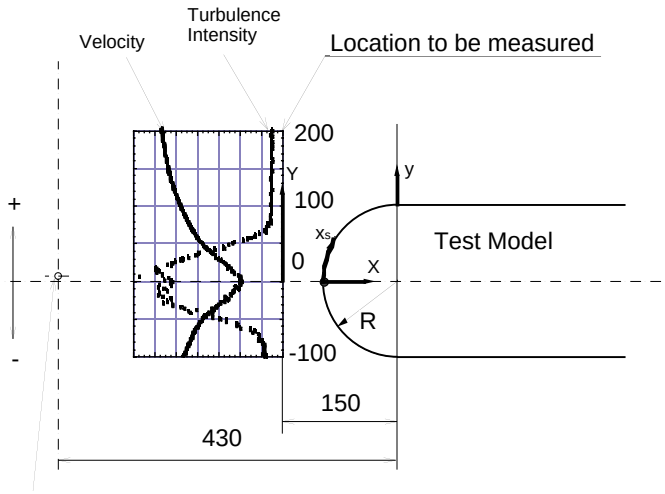

Figure 10 Schemetic showing the relationship between the wake-generating bar and the test model

turbulence intensity in the shear layer increased until the height of the high turbulence zone reached a maximum at $x_s/R \cong 1.7$. Thereafter, due to its inherently unstable characteristics, the shear layer eventually broke down into turbulence and the streamlines bent towards the wall, resulting in the reattachment of the shear layer at $x_s/R \cong 1.9$. Comparing the two cases of $i = 0$ and $i = 5$, it follows that the maximum height of the shear layer was larger for $i = 5$ than for $i = 0$, and that the transverse extent of the highly turbulent region was also wider for $i = 5$. This made the boundary layer thicker, as will be discussed later.

Boundary Layer Thickness Figure 8 shows displacement and momentum thicknesses over the model surface obtained for five incidence cases. The displacement thickness for each incidence attained the extreme at $x_s/R \cong 1.7$ due to the blockage effect of the separation bubble, followed by a decrease until the reattachment point. Then the displacement thickness began to increase again in an almost linear manner. The incidence $i = 5$ yielded the largest displacement thickness among the tested conditions, which was also the case for the momentum thickness. The momentum thicknesses gradually increased until $x_s/R \cong 1.7$, remaining almost the same level for all the incidences. Thereafter their rates of increase began to differ with i and the momentum thicknesses became different from one to another. In consideration of the fact that momentum thickness is determined by wall shear stress through the momentum-integral equation (Schlichting(1979)), the observed momentum thicknesses indicated that the transitional behaviors of the shear layers differed, resulting in the difference of the wall shear stresses.

Two-Dimensionality Figure 9 demonstrates a comparison of the velocity profiles measured at 50mm-separated locations by use of the two probes as shown in Figure 5. The two velocity profiles at each location almost agreed with each other, although slight differences appeared inside the separation bubble due to its three-dimensional characteristics. Further comparisons of velocity and turbulence intensity profiles with or without the influence of the bar-wake were executed, which concluded that the boundary layer on the test model sustained satisfactory two-dimensionality at least over the measurement domain.

Bar-Wake Measurements

Prior to the measurements of wake-affected boundary layers, pro-

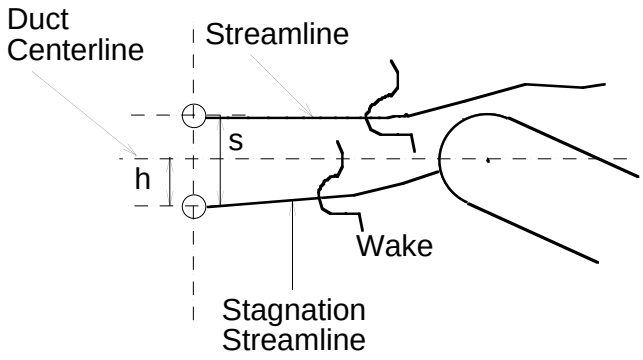

Figure 11 Schemetic showing the relationship between the wake-generating bar and the test model

Table 1 Values of h for three incidences

	i = -5	i = 0	i = 5
h [mm]	45	6	-5

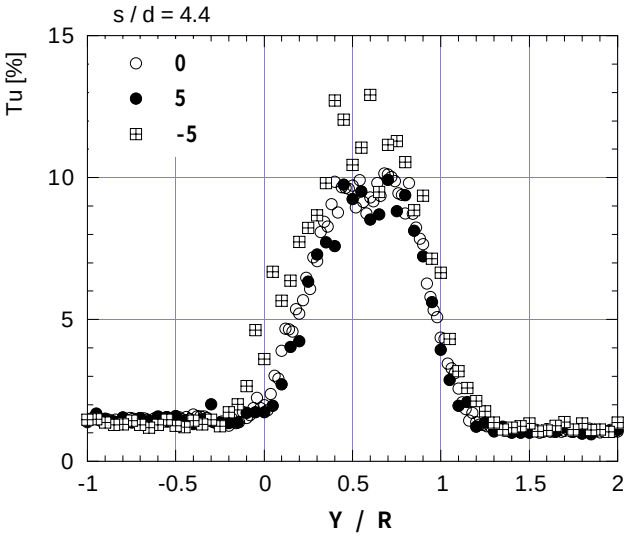

Figure 12 Wake turbulence profiles for three incidences (s/d = 4.4)

files of velocity and turbulence intensity in the incoming bar-wake for several incidences of the test model were acquired, as shown in Figure 10. The measured location was 0.05 [m] upstream of the model leading edge. These measurements, by changing the bar position, also provided a rough estimation on the location of the stagnation streamline against the test model for each of the incidences. The detected location of the stagnation streamline was referred to in terms of h: the distance between the stagnation streamline and the duct centerline as illustrated in Figure 11. Table 1 presents the values of h obtained for three incidences. As seen in the pressure distributions (Figure 6), the stagnation streamline for i = 0 did not coincide with the duct centerline (h = 0). When the bar was 'clocked', in other words, moved in the vertical direction, its location was measured from the stagnation stream line for each incidence. Figure 12 depicts the wake turbulence profiles of the clocked (s/d =4.4) bars measured at the three incidence cases. These data shows that the vertical extent of the wake

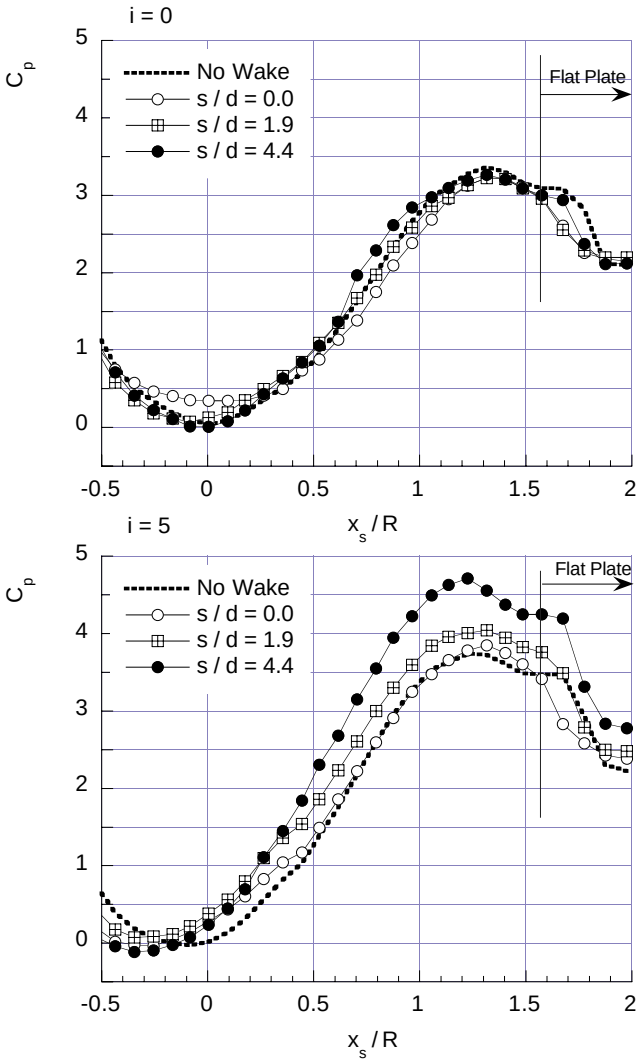

Figure 13 Wake-affected pressure distributions (upper : i = 0 , lower : i = 5)

was about the radius of the model leading edge.

Effects of the Bar-Wake

Pressure Distributions Figures 13 shows wake-affected pressure distributions over the test model for the cases of i = 0 and i = 5, where the bar located at three vertical positions to examine the clocking effects on separated boundary layers. The bar-wake at s/d =0.0 covered the stagnation region on the model leading edge, hence the pressure coefficients near the stagnation point exhibited non-zero values. Downstream of the stagnation region, the pressure coefficients tended to decrease in comparison with the data of no wake condition, which indicated the flow deceleration due to the incident wake. The separation bubble almost disappear under this condition. When the bar was at s/d =1.9, the wake-affected pressure distribution agreed with the undisturbed one, except for the diminished separation bubble. Shifting the bar to a further upward position (s/d =4.4), the pressure distribution recovered from the wake-affected state. However, the flow velocity increased over the region x_s/R = 0.6 - 1.0 compared to the no wake data due to the displacement effect of the bar wake, and the separation bubble was still shorter than the undisturbed separation bubble. The bar-wake for i = 5 induced more noticeable change in the pressure distribution than that of i = 0. Especially, the data of s/d =4.4

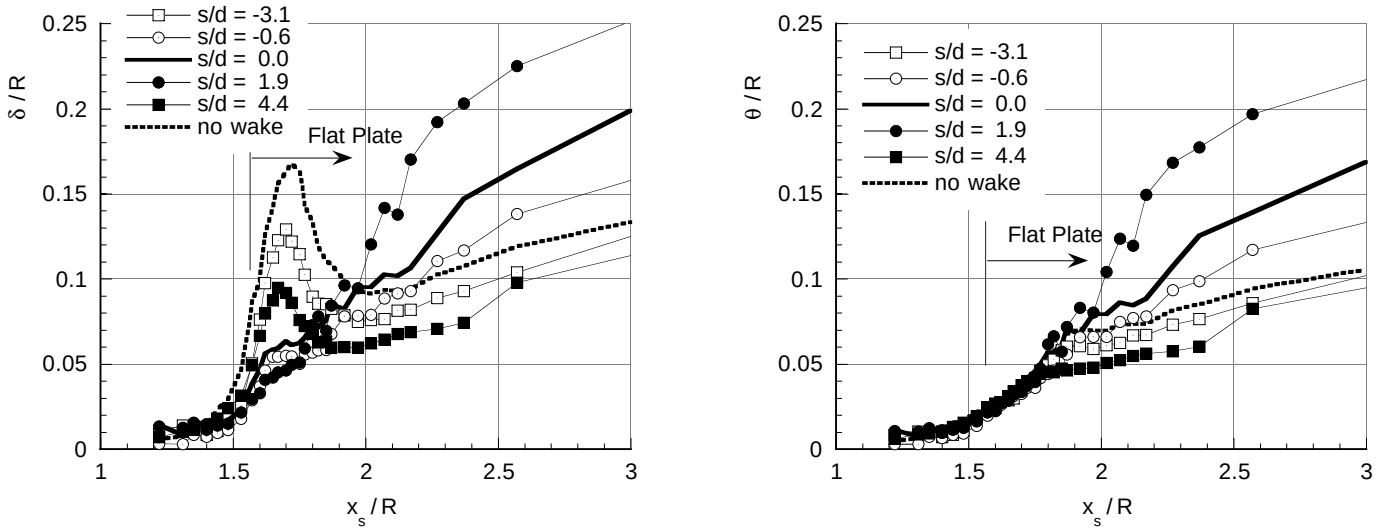

Figure 14 Wake-affected displacement thickness and momemtum thickness for i = 0 (left : displacement thickness right : momentum thickness)

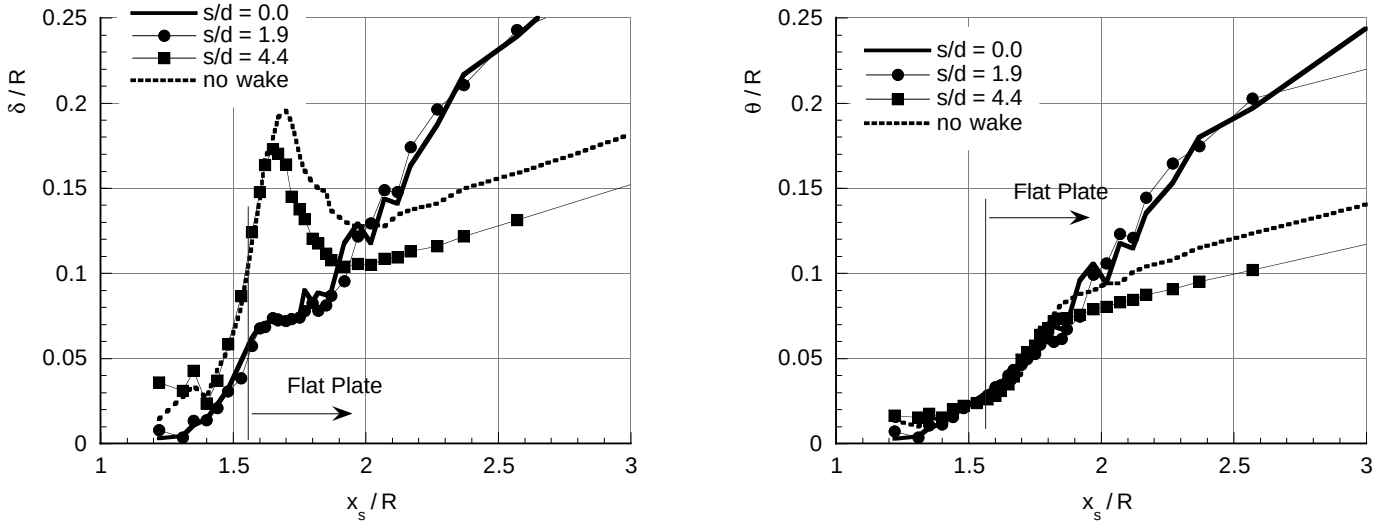

Figure 15 Wake-affected displacement thickness and momemtum thickness for i = 5 (left : displacement thickness right : momentum thickness)

indicated that the flow over the model leading edge was considerably accelerated due to the wake effect. The separation bubble became obscure in the data for s/d =0.0 and 1.9.

Boundary Layer Thickness Figures 14 - 16 show wake-affected boundary layer thicknesses for three incidence cases.

In Figure 14 one can examine the bar-clocking effect upon the displacement and momentum thicknesses for i = 0. When the bar situated near the stagnation streamline (s/d = 0.0, 1.9 or -0.6), the displacement thickness exhibited no peak where the separation bubble had existed in no wake condition. This was because the bar-wake disturbed the boundary layer in such a drastic manner from the stagnation point that the boundary layer was able to keep attached against the adverse pressure gradient that appeared over x_s/R = 1.4 - 1.8, resulting in the extinction of the separation bubble. The velocity profiles or turbulence intensity distribution shown in the upper data of Figure 17 confirmed the above-mentioned explanation. The rapid increase in the displacement thickness after the adverse pressure gradient zone seemed to originate from the faster completion of the boundary layer transition due to high production rate of turbulent spots rate under the adverse pressure gradient as well as highly disturbed main flow. The momentum thickness also grew rapidly in accordance with the displacement thickness. The observed increase in the momentum thickness suggested the intensely enhanced wall shear stress in this case. When the bar was located further upward (s/d = 4.4), the corresponding displacement thickness clearly indicated the existence of a restoring separation bubble, which could be confirmed by looking at the velocity profiles or the peak positions of the turbulence intensity as shown in the lower data of Figure 17. It is worthy to note that the momentum thickness under the influence of the bar wake at s/d = 4.4 became meaningfully smaller than that of the no wake condition. This implies a possibility that the aerodynamic penalty associated with the separation bubble might be reduced to some extent by the introduction of a properly ‘clocked’ stationary wake, which will be discussed later in this paper.

Figure 15 shows the wake-affected displacement and momentum thicknesses for i = 5. Likewise in the previous case, the bar wake at s/d = 4.4 influenced the boundary layer so that its displace-

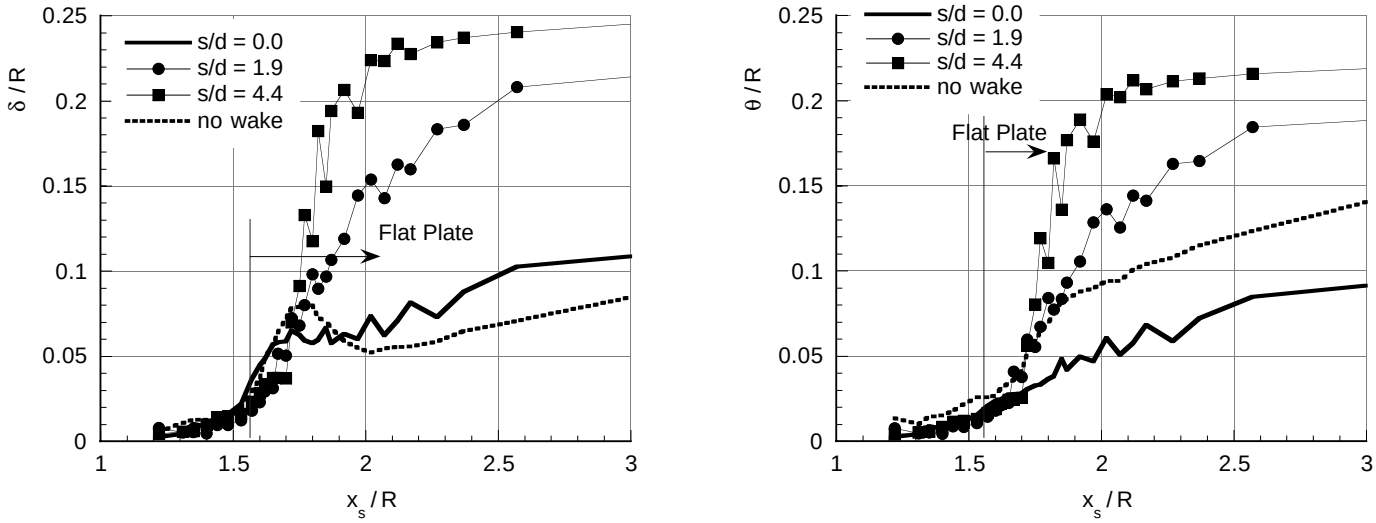

Figure 16 Wake-affected displacement thickness and momemtum thickness for i = -5 (left : displacement thickness right : momentum thickness)

ment and momentum thicknesses meaningfully reduced in comparison with those of the boundary layer for no wake condition. From the comparison of the velocity profiles and the turbulence intensities between wake-affected condition (Figure 18) and the no wake condition (Figure 7), however, one can notice that the size of the separation bubble remained almost unchanged even under the influence of the incident wake. This implies that the observed reduction in the boundary layer thicknesses was mainly due to the wake-induced flow acceleration as seen in Figure 13, while the effect of the wake turbulence remained secondary. For the negative incidence (i = -5), where the separation bubble over the test surface became relatively small, the bar wake induced significant increases in the boundary layer thicknesses when the bar situated at s/d = 1.9 or s/d = 4.4, while the wake at s/d = 0.0 caused the reduction of the momentum thickness.

Discussions

According to Denton (1993), loss generated in the boundary layer is proportional to the product of boundary layer energy dissipation thickness times the cube of local velocity. Thus we defined the following parameter as an index of the loss, that is

$$\zeta = \left(U/U_{in}\right)^3 \delta_3 \ . \qquad (8)$$

Figure 19 shows the loss indices over the test surface for the three incidences. For most of the test cases except for s/d = 4.4 at i = 0 or s/d = 0.0 at i = -5, the introduction of the upstream stationary wake brought about no aerodynamic benefits but considerable losses. For the two exceptional cases, especially s/d = 4.4 at i = 0, the values of the loss index became lower than those of no wake condition. In order to make a more appropriate evaluation of the stationary wake effect upon the aerodynamic performance of the blade, however, it is necessary to examine the effects of moving wakes, which was not taken into account in the present study. Nevertheless, the above-mentioned results indicate a possibility that the aerodynamic loss due to a boundary layer accompanying separation bubble can be reduced if a circumferential position of wake-generating obstacle is properly chosen with respect to a target blade.

Conclusions

This paper examined how upstream stationary wake from the cylindrical bar , which was transversely ‘clocked’, affected the characteristics of separation bubble on the large-scaled test model. Boundary layer measurements through the hot-wire probe revealed that there was a possibility for reducing the aerodynamic loss associated with the boundary layer by choosing a proper position of the bar against the model.

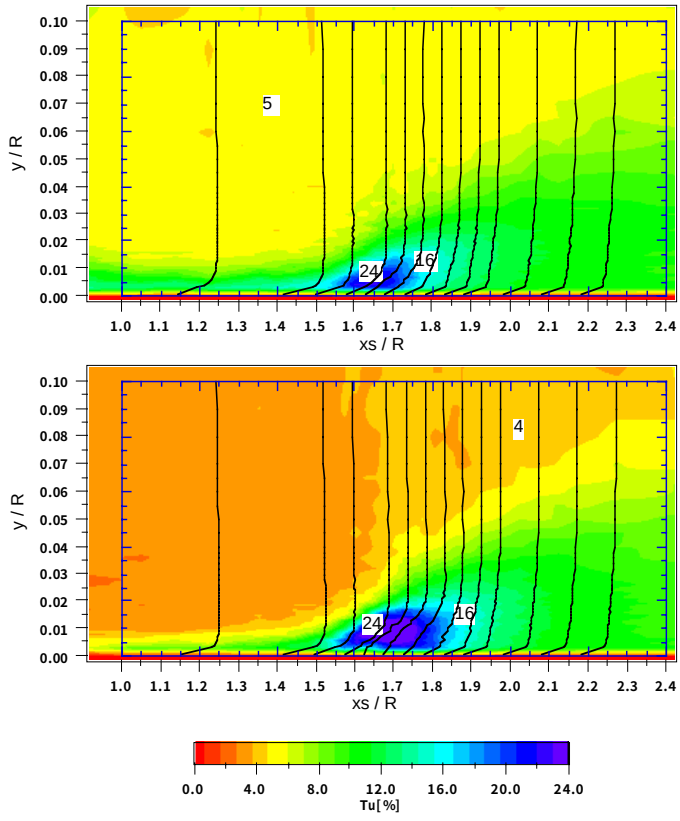

Figure 17 Wake-disturbed velocity profiles and turbulence intensity contours for i = 0 upper : s/d = 0 / lower : s/d = 4.4

Acknowledgment

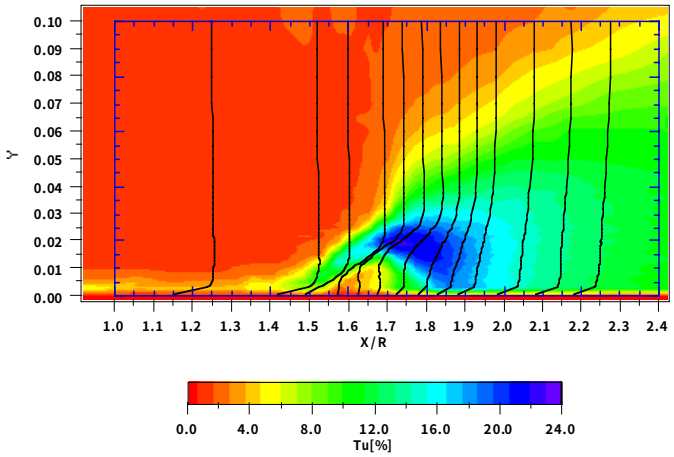

Figure 18 Wake-disturbed velocity profiles and turbulence intensity contours for i = 5 and s/d = 4.4

The authors are greatly indebted to Messrs. K. Takahashi and T. Tsuchimine for their invaluable efforts to construct the experimental system.

References

Calvart, W. J., 1994, "An Inviscid-Viscous Method to Model Leading Edge Separation Bubbles," ASME Paper 94-GT-385.

Cumpsty, N. A., 1989, "Compressor Aerodynamics," Longman Scientific & Technical.

Cumpsty, N. A., Dong, Y. and Li, Y. S., 1995, "Compressor Blade Boundary Layers in the Presence of Wakes," ASME Paper 95-GT-443.

Denton, J. D., 1993, “Loss Mechanisms in Turbomachines,” Journal of Turbomachinery, Vol. 115, pp. 621-656.

Dorney, D. J., 1998, "Physics of Airfoil Clocking in a High-Speed Axial Compressors," ASME Paper 98-GT-82.

Funazaki, K., Tetsuka, N. and Tanuma, T., 1999, "Effects of Periodic Wake Passing upon Aerodynamic Loss of a Turbine Cascade.

Part I: Measurements of Wake-Affected Cascade Loss by Use of a Pneumatic Probe," ASME Paper 99-GT-93.

Griffin, L. W., Huber, F. W. and Sharma, O. P., 1996, "Performance Improvement Through Indexing of Turbine Airfoils: part 2 - Numerical Simulation," Trans. ASME Journal of Turbomachinery, Vol. 118, pp. 636-642.

Gundy-Burlet, K. L. and Dorney, D. J., 1997, "Physics of Airfoil Clocking in Axial Compressors," ASME Paper 97-GT-444.

Hazarika, B. K. and Hirsch, C., 1994, "Behavior of Separation Bubble and Reattached Boundary Layer around a Circular Leading Edge," ASME Paper 94-GT-385.

Hazarika, B. K. and Hirsch, C., 1995, "Transition over C4 Leading Edge and Measurement of Intermittency Factor Using PDF of Hot-Wire Signal," ASME Paper 95-GT-294.

Hazarika, B. K. and Hirsch, C., 1996, "The Effect of Reynolds Number on the Behavior of a Leading Edge Separation Bubble," ASME Paper 96-GT-410.

Huber, F. W., Johnson, P. D., Sharma, O. P., Staubach, J. B. and Gaddis, S. W., 1996b, "Performance Improvement Through Indexing of Turbine Airfoils: Part 1 - Experimental Investigation," Trans. ASME Journal of Turbomachinery, Vol. 118, pp. 630-635.

Kyriakides, N.K., Kastrinakis, E.G., Nychas, S.G., and Goulas, A., 1999, "Aspects of Flow Structure during a Cylinder Wake-Induced Laminar/Turbulent Transition," AIAA Journal, Vol. 37, No. 10,

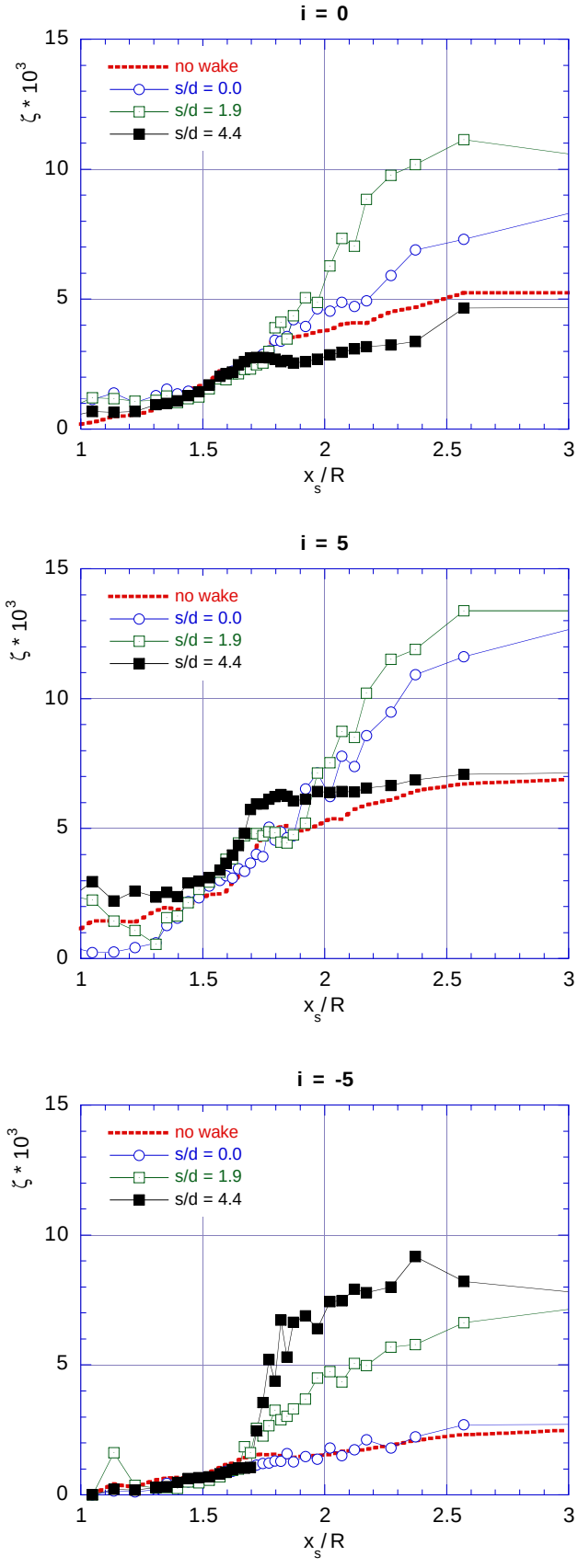

Figure 19 Effect of the bar wake on loss generation within the boundary layer

pp.1197-1205.

Malkiel, E. and Mayle, R. E., 1995, "Transition in a Separation Bubble," ASME Paper 95-GT-32.

Schlichting, H., 1979, "Boundary-Layer Theory," McGraw-Hill.

Schulte, V. and Hodson, H. P., 1998, "Prediction of the Becalmed Region for LP Turbine Profile Design," Trans. ASME Journal of Turbomachinery, Vol. 120, pp. 839-846.

Walraevens, R. E. and Cumptsy, N. A., 1995, "Leading Edge Separation Bubbles on Turbomachines Blades," Trans. ASME Journal of Turbomachinery, Vol. 117, pp. 115-125.